

# A Novel Two-Dimensional Sparse-Weight NLMS Filtering Scheme for Passive Bistatic Radar

Yahui Ma, *Student Member, IEEE*, Tao Shan, *Member, IEEE*, Yimin D. Zhang, *Senior Member, IEEE*, Moeness G. Amin, *Fellow, IEEE*, Ran Tao, *Senior Member, IEEE*, and Yuan Feng

**Abstract**—In passive bistatic radars, weak target echoes may often be masked by direct path interference, multipath components, and strong target echoes, making weak target detection a challenging problem. The conventional 1-D adaptive cancellation algorithms, such as the normalized least mean square (NLMS), cannot effectively suppress strong target echoes when their Doppler frequencies spread. In addition, the continuous distribution of the NLMS weight vector does not match the sparse characteristics of strong multipath components and target echoes, thus resulting in degraded cancellation performance. Motivated by this fact, a novel 2-D sparse-weight NLMS filtering scheme is proposed by extending the NLMS to a 2-D structure, in which the weight vector is sparsely distributed and adaptively adjusted based on the sparse strong multipath components and target echoes.

**Index Terms**—Passive bistatic radar (PBR), sparse weights, 2-D adaptive filter.

## I. INTRODUCTION

WITH the advantages of low cost, covert operation, low vulnerability, and reduced impact on the environment, passive bistatic radar (PBR) has attracted considerable and increasing interests in recent years. Because of the random nature of the transmitted waveform, however, the sidelobes of its ambiguity function have a time-varying structure, and their peak levels may approach the main-lobe level [1]–[3]. This causes problems such that weak target echoes are masked by strong clutter, which includes both direct path interference (DPI) and stationary multipath components, and strong echoes from other targets [4], [5].

Various approaches have been proposed to solve this problem. Adaptive cancellation algorithms, such as recursive least square, normalized least square (NLMS), and Wiener

Manuscript received May 12, 2015; revised September 18, 2015 and February 11, 2016; accepted February 21, 2016. Date of publication March 17, 2016; date of current version April 20, 2016. The work of Y. Ma, T. Shan, R. Tao, and F. Yuan was supported in part by the National Natural Science Foundation of China under Grants 61331021, 61421001, 61172176, and 61490691. The work of Y. D. Zhang and M. G. Amin was supported in part by the National Science Foundation under Grant EARS-1547420. The work of T. Shan was supported by the China Scholarship Council.

Y. Ma, T. Shan, R. Tao, and Y. Feng are with the School of Information and Electronics, Beijing Institute of Technology, Beijing 100081, China, and also with Beijing Key Laboratory of Fractional Signals and Systems, Beijing 100081, China (e-mail: shantao@bit.edu.cn).

Y. D. Zhang is with the Department of Electrical and Computer Engineering, College of Engineering, Temple University, Philadelphia, PA 19122 USA.

M. G. Amin is with the Center for Advanced Communications, Villanova University, Villanova, PA 19085 USA.

Color versions of one or more of the figures in this paper are available online at <http://ieeexplore.ieee.org>.

Digital Object Identifier 10.1109/LGRS.2016.2535173

algorithms, are commonly used methods for interference suppression in PBR [6]–[8]. These algorithms are 1-D high-pass filters that only effectively suppress clutter and interference with a zero Doppler frequency. On the other hand, several approaches were proposed to cancel clutter and interference with nonzero frequencies. An iterative approach was proposed in [4] and [5] to cancel strong multipath components and other target echoes in a progressive manner. A sequential cancellation algorithm was presented in [9] to adaptively determine the number of iterations based on the measured data. Furthermore, an extensive cancellation algorithm was proposed to solve the masking effect [10]. Recently, a multistage procedure [11] and a multifrequency estimation notch filter [12] are presented to achieve the low-complexity cancellation of strong echoes. However, all these algorithms do not take advantage of the sparse characteristic of multipath components.

The authors have proposed an adaptive discrete NLMS algorithm to cancel sparse multipath components [13]. This algorithm, however, does not effectively suppress strong target echoes. A multichannel NLMS (MCNLMS) algorithm was recently proposed to suppress clutter with nonzero Doppler frequencies [14]. The weight vector assumes a continuous distribution, which does not match the sparse characteristics of the multipath components and strong target echoes. In addition, filters with continuous weight vectors may yield the undesirable cancellation of weak target signals. In this letter, we develop a novel 2-D sparse-weight NLMS (TD-SWNLMS) filtering scheme that effectively suppresses both sparse multipath components and strong target echoes. The effectiveness of the proposed scheme is verified using real data experiment.

This letter is organized as follows. The signal model is described in Section II. The TD-SWNLMS filtering scheme is derived in Section III. In Section IV, the effectiveness of the algorithms is demonstrated using real data. Finally, conclusions are drawn in Section V.

## II. SIGNAL MODEL

Fig. 1 shows the PBR geometry, where the reference antenna receives the reference signal directly from the transmitter, which is modeled in the baseband as

$$u(n) = A_{\text{refr}} s(n) + n_{\text{refr}}(n) \quad (1)$$

where  $A_{\text{refr}}$  and  $s(n)$  are the amplitude and the discretized waveform of the reference signal, respectively, and  $n_{\text{refr}}(n)$  is the additive noise. The surveillance antenna receives the echo

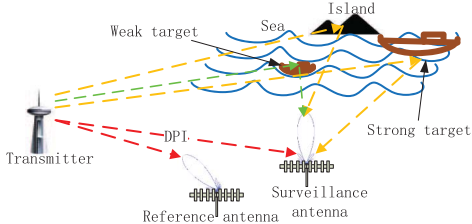


Fig. 1. PBR geometry.

signal, which consists of DPI, strong multipaths, and target echoes, and can be modeled as

$$\begin{aligned} y(n) = & A_{\text{echo}} s(n) + \sum_{i=1}^{M_P} a_i s(n - k_i) \\ & + \sum_{m=1}^{M_T} b_m s(n - l_m) e^{\frac{j2\pi n f_m}{f_s}} + n_{\text{echo}}(n) \quad (2) \end{aligned}$$

where  $A_{\text{echo}}$  is the complex gain of the DPI received from the sidelobes of the surveillance antenna and  $M_P$  and  $M_T$  are the numbers of multipath components and targets, respectively. In addition,  $a_i$  and  $k_i$  are the complex amplitude and time delay of the  $i$ th multipath, respectively, and  $b_m$ ,  $l_m$ , and  $f_m$  denote the complex amplitude, time delay, and Doppler frequency of the  $m$ th target, respectively. Furthermore,  $f_s$  stands for the sampling rate, and  $n_{\text{echo}}(n)$  represents the thermal noise.

Representing the third term in the right-hand side of (2) in terms of strong and weak target terms yields

$$\begin{aligned} y(n) = & A_{\text{echo}} s(n) + \sum_{i=1}^{M_P} a_i s(n - k_i) \\ & + \sum_{p=1}^{M_S} w_{\star p} s(n - l_{\star p}) e^{\frac{j2\pi n f_{\star p}}{f_s}} \\ & + \sum_{q=1}^{M_W} w_{\diamond q} s(n - l_{\diamond q}) e^{\frac{j2\pi n f_{\diamond q}}{f_s}} + n_{\text{echo}}(n) \quad (3) \end{aligned}$$

where  $M_S$  and  $M_W$  are the numbers of strong and weak targets, respectively. Let  $M_T = M_S + M_W$ . In addition,  $w_{\star p}$ ,  $l_{\star p}$ , and  $f_{\star p}$  denote the complex amplitudes, time delay, and Doppler frequency of the  $p$ th strong target, respectively, and  $w_{\diamond q}$ ,  $l_{\diamond q}$ , and  $f_{\diamond q}$  respectively represent the complex amplitudes, time delay, and Doppler frequency of the  $q$ th weak target.

### III. TD-SWNLMS FILTERING SCHEME

Denote DPI, multipath components, and strong target echoes as  $d_a(n)$ ,  $d_c(n)$ , and  $d_p(n)$ , respectively. They are collectively referred to as interference component, and its estimate is expressed as

$$\hat{y}(n) = \hat{d}_a(n) + \hat{d}_c(n) + \hat{d}_p(n). \quad (4)$$

According to (3),  $\hat{d}_a(n)$  and  $\hat{d}_c(n)$  can be estimated by convolving the reference signal with a discrete weight vector, and  $\hat{d}_p(n)$  can be estimated by convolving the frequency-modulated reference signal with a discrete weight vector. The output residual

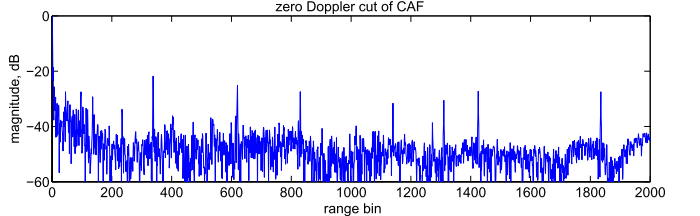


Fig. 2. Distribution of multipath components before cancellation.

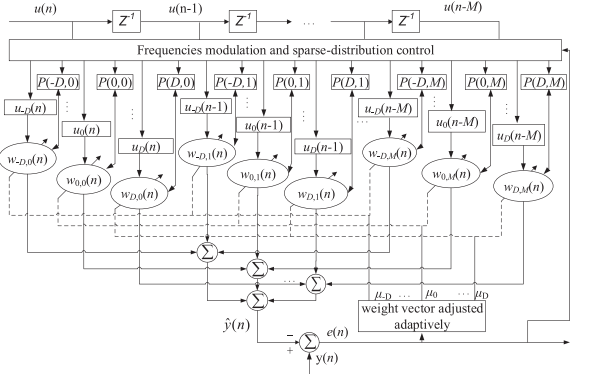


Fig. 3. Schematic diagram of the proposed method.

of the filter after interference suppression, which contains the desired echo signal, can be expressed as

$$e(n) = y(n) - \hat{y}(n). \quad (5)$$

In some applications, e.g., sea surface target detection, isolated strong scatterers from stationary objects, such as distant mountains, islands, and cays, often lead to clutter components that are sparse in range (i.e., time delay). Fig. 2 demonstrates such sparse characteristics of multipath signals with an example of the zero-Doppler cut of the cross-ambiguity function (CAF) obtained from digital television (DTV)-based experimental PBR. It can be clearly seen that only a small part of the clutter components are strong. In order to cancel both sparse multipath components and strong target echoes, the traditional 1-D (time delay only) NLMS filter structure should be extended to a 2-D (time delay and Doppler frequency) structure. However, the use of all filter weights requires a high complexity and causes two problems: 1) The steady-state clutter cancelation performance is degraded since the error of the filter output increases with its length [8], and 2) it may cancel weak target echoes when they share the same Doppler frequency with strong targets.

Motivated by the aforementioned facts, a novel 2-D sparse-weight adaptive filter structure is proposed. In the schematic diagram shown in Fig. 3,  $u(n)$  is the input signal at time  $n$ , and  $M$  is the maximum length of the filter delays. In addition,  $P$  denotes a  $(2D+1) \times (M+1)$  sparse weight support matrix, whose elements take binary values. Denote  $D$  as the maximum Doppler bin of targets. The position  $(d, m)$  with nonzero element  $P(d, m)$  corresponds to a sparse weight, where  $d \in [-D, D]$  is the Doppler bin representing the Doppler frequency  $d/T$ ,  $T$  is the coherent integration time, and  $m \in [0, M]$  is the time delay bin representing the time delay  $m/f_s$ . In addition,  $\mu_d$ ,  $u_d(n-m) = u(n-m)e^{j2\pi(n-m)d/N}$ , and  $w_{d,m}(n)$  denote the step size, a sparse tap input value, and its corresponding

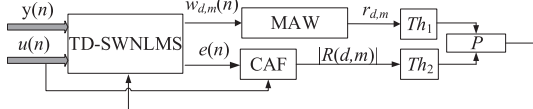


Fig. 4. Flow diagram of signal processing procedure.

weight in Doppler bin  $d$ , respectively, where  $N = Tf_s$ . Define  $\bar{\mathbf{w}}_d(n) = [w_{d,0}(n), w_{d,1}(n), \dots, w_{d,M}(n)]^T$  and  $\bar{\mathbf{u}}_d(n) = [u_d(n), u_d(n-1), \dots, u_d(n-M)]^T$  as the weight vector and the input signal vector corresponding to the  $d$ th Doppler bin, respectively, where superscript  $(\cdot)^T$  denotes transpose.

An important consideration in the TD-SWNLMS filter design is to optimize matrix  $P$  such that its nonzero entries correspond to the positions of the multipath components and strong target echoes. The matrix  $P$  is updated based on the weight vectors and CAF. The flow diagram of the signal processing procedure is shown in Fig. 4, where MAW stands for the mean accumulated weight value and  $Th_1$  and  $Th_2$  are respective thresholds for the sparse weights and the strong echoes from multipath components and strong targets.

The update process of the filter weight vector is described as follows.

**Initialization:** All elements in the zeroth row of matrix  $P$  are set to 1, whereas elements in the other rows are set to 0.

### Step 1: Adaptive cancellation.

Use the TD-SWNLMS filter to cancel the DPI, multipath components, and strong target echoes. The estimation of  $y(n)$  is expressed as

$$\hat{y}(n) = \sum_{d=-D}^D \sum_{m=0}^M P(d, m) w_{d,m}^*(n) u_d(n-m) \quad (6)$$

where superscript  $(\cdot)^*$  denotes the complex conjugate.

Compute the sparse weight vector based on the following updated equation for  $d = -D, \dots, D$  (the derivation is provided in the Appendix):

$$\mathbf{w}_d(n+1) = \mathbf{w}_d(n) + \frac{\mu_d}{\lambda' + \sum_{d=-D}^D \mathbf{u}_d^H(n) \mathbf{u}_d(n)} \mathbf{u}_d(n) e^*(n) \quad (7)$$

where  $\mathbf{w}_d(n) = \mathcal{P}_d \odot \bar{\mathbf{w}}_d(n)$  and  $\mathbf{u}_d(n) = \mathcal{P}_d \odot \bar{\mathbf{u}}_d(n)$  are the weight vector and its associated input vector corresponding to the  $d$ th Doppler bin, respectively,  $\mathcal{P}_d = [P(d, 0), P(d, 1), \dots, P(d, M)]^T$  denotes the sparse weight support vector,  $\odot$  represents the elementwise multiplication,  $\lambda'$  is a small positive value to avoid overflow, and superscript  $(\cdot)^H$  denotes the conjugate transpose.

It is observed from (6) and (7) that the sparse characteristics of the TD-SWNLMS filter are mainly reflected in the sparsity of the weight vectors. The continuous weight vectors are sparsified by multiplying a sparse basis vector  $\mathcal{P}_d$ , which is derived by two criteria respectively based on MAW and CAF. The sparse weight vector can be updated adaptively to match the sparse clutter components and strong target echoes.

### Step 2: Remove small-value weights.

Define MAW as

$$r_{d,m} = \frac{1}{N'} \sum_{n=N-N'+1}^N |w_{d,m}(n)| \quad (8)$$

where  $N'$  is the length of accumulation. Small-value weights are removed by letting

$$P(d, m) = 0, \quad \forall r_{d,m} < Th_1 \quad (9)$$

where the threshold is set to  $Th_1 = \max(r_{d,m}) \cdot \eta$ ,  $\eta = 1/\sqrt{\text{SNR}_1 \cdot \alpha}$  is a threshold coefficient,  $\text{SNR}_1 = |\sum_{n=1}^N u^*(n)y(n)|^2 / (N E\{|\sum_{n=1}^N u^*(n)e(n+l)e^{-j2\pi dn/N}|^2\})$  is the signal-to-noise ratio (SNR) of the DPI,  $(d, l)$  is the position of the CAF sidelobes,  $E\{\cdot\}$  denotes statistical expectation, and  $\alpha$  is a constant to be selected based on prior information to obtain a high SNR. It can be concluded from (9) that only weights with small values will be removed.

### Step 3: Add weights corresponding to strong target echoes and uncanceled multipath components.

First, compute the discrete-time CAF as

$$R(d, l) = \sum_{n=1}^N u^*(n)e(n+l)e^{-j2\pi dn/N} \quad (10)$$

where  $l \in [0, L]$ ,  $L \geq M$ , and  $L$  is the maximum time delay bin of targets. Then, sparse weights and their support corresponding to uncanceled multipath components and strong target echoes are added by letting

$$w_{d,m}(n) = \frac{R(d, m)}{R_0}, \quad P(d, m) = 1, \quad \forall |R(d, m)| > Th_2 \quad (11)$$

where  $R_0 = \sum_{n=1}^N |u(n)|^2$ ,  $Th_2 = \delta_n \cdot \rho$ , and  $\delta_n$  is the noise floor which can be estimated over a portion of the CAF surface where targets are absent. In addition,  $\rho = \sqrt{\text{PSLR}/\alpha}$  is a positive coefficient used to control the threshold, and  $\text{PSLR} = |\sum_{n=1}^N |u(n)|^2|^2 / E\{|\sum_{n=1}^N u^*(n)u(n+l_s)e^{-j2\pi d_s n/N}|^2\}$  is the peak-to-sidelobe ratio (PSLR), where  $(d_s, l_s)$  is the position of the sidelobe in the autoambiguity function of the reference signal. It is clear that element  $P(d, m)$  corresponding to strong target echoes or uncanceled multipath components will be set to 1, and  $P$  is updated only once for every data segment.

**Repeat steps 1 to 3** for every data segment with  $n = (i-1)N+1 : iN$  for  $i = 1, 2, \dots$ , until  $iN = \mathcal{N}$ , where  $\mathcal{N}$  is the total length of the data.

## IV. REAL DATA VERIFICATION

A real data set, which was collected by using a DTV-based PBR system with a baseband sampling rate of 10 MHz, is used in the following analysis. Fig. 5 shows the experimental environment at the east coast of China, where two double-row Yagi antennas are used, one receiving the reference signal and the other receiving echo signals. The carrier frequency of the transmitted DTV signal is 746 MHz, and the bandwidth is 7.56 MHz. The coherent integration time is 0.2 s. Therefore, the yielded data segment contains  $2 \times 10^6$  samples, and the Doppler resolution is 5 Hz. The estimated input  $\text{SNR}_1$  is 59.33 dB, and the measured PSLR is about 60 dB.

Fig. 6(a) and (b) shows the CAF maps after canceling the DPI and multipath components by using the NLMS algorithm,



Fig. 5. Experimental environment.

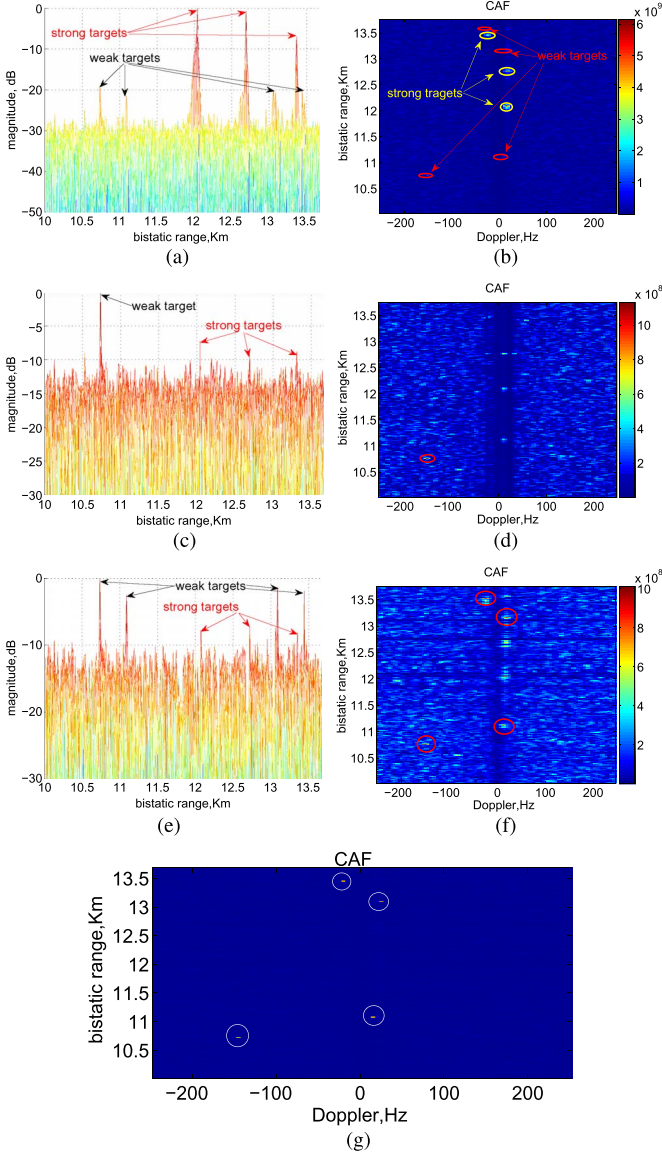


Fig. 6. CAF maps. (a) Range profile using NLMS. (b) Range-Doppler plot using NLMS. (c) Range profile using MCNLMS. (d) Range-Doppler plot using MCNLMS. (e) Range profile using TD-SWNLMS. (f) Range-Doppler plot using TD-SWNLMS. (g) Range-Doppler plot of CFAR detector using TD-SWNLMS.

where the step size of  $\mu = 0.01$  and the filter length of  $M = 2000$  are determined based on the maximum range of clutter. The measured Doppler frequencies, bistatic ranges, and signal-

TABLE I  
MEASURED TARGET SINR IN DECIBELS

target	S1	S2	S3	W1	W2	W3	W4
SINR <sub>sc</sub>	32.53	31.26	25.58	12.88	12.06	12.13	11.64
SINR <sub>mc</sub>	6.6	6.49	6.33	14.21	5.08	5.40	6.13
SINR <sub>ms</sub>	7.74	6.85	6.36	14.66	13.86	14.06	13.54

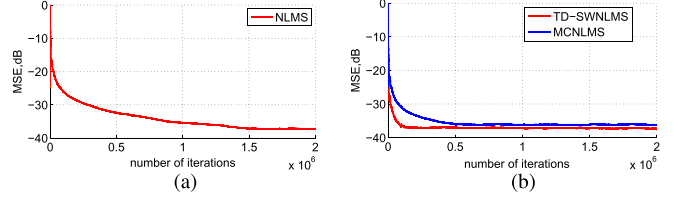


Fig. 7. Convergence curves. (a) First data segment. (b) Second data segment.

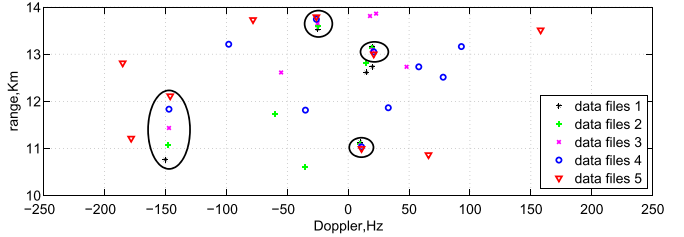


Fig. 8. Superposition of detection results over data file sequence obtained by using TD-SWNLMS.

to-interference-plus-noise ratios (SINRs) (denoted as  $\text{SINR}_{sc}$  in Table I) of the three strong targets are S1 ( $-25 \text{ Hz}, 13.45 \text{ km}$ , and  $32.53 \text{ dB}$ ), S2 ( $15 \text{ Hz}, 12.1 \text{ km}$ , and  $31.26 \text{ dB}$ ), and S3 ( $20 \text{ Hz}, 12.76 \text{ km}$ , and  $25.58 \text{ dB}$ ), and those for the four weak targets are W1 ( $-150 \text{ Hz}, 10.76 \text{ km}$ , and  $12.88 \text{ dB}$ ), W2 ( $15 \text{ Hz}, 11.13 \text{ km}$ , and  $12.06 \text{ dB}$ ), W3 ( $20 \text{ Hz}, 13.16 \text{ km}$ , and  $12.13 \text{ dB}$ ), and W4 ( $-25 \text{ Hz}, 13.53 \text{ km}$ , and  $11.64 \text{ dB}$ ). Assume a minimum detectable SINR to be  $13 \text{ dB}$ . In this case, the NLMS filter fails to detect the weak targets.

For the MCNLMS filter, the parameters used are  $K = 4$ ,  $f_1 = 0 \text{ Hz}$ ,  $f_2 = -25 \text{ Hz}$ ,  $f_3 = 15 \text{ Hz}$ ,  $f_4 = 20 \text{ Hz}$ ,  $M = 2000$ ,  $\mu_1 = 0.01$ , and  $\mu_{2:4} = 0.007$ . The results are shown in Fig. 6(c) and (d). From the output  $\text{SINR}_{mc}$  depicted in Table I, the MCNLMS effectively cancels strong targets. However, it suppresses weak targets as well, yielding their low SINRs.

Fig. 6(e)–(g) shows the resulting CAF maps when the TD-SWNLMS algorithm is used, where the parameters are set as  $L = 2000$ ,  $N' = 5 \times 10^5$ ,  $M = 2000$ ,  $D = 30$ , and  $\alpha = 1000$ . The yielded target  $\text{SINR}_{ms}$  results clearly show that the three strong targets are canceled and the four weak targets achieve high SINRs of  $14.66$ ,  $13.86$ ,  $14.06$ , and  $13.54 \text{ dB}$ , respectively.

The convergence curve of the first data segment is shown in Fig. 7(a). It is evident that the filter reaches a steady state after about  $1.5 \times 10^5$  iterations. Starting from the second data segment, as shown in Fig. 7(b), the TD-SWNLMS filter achieves a faster convergence rate and a smaller steady-state error as compared to the MCNLMS filter.

Fig. 8 shows the detection results obtained from five data files, each with a 5-s interval. The four weak targets are confirmed as those consistently observed from all data sets.

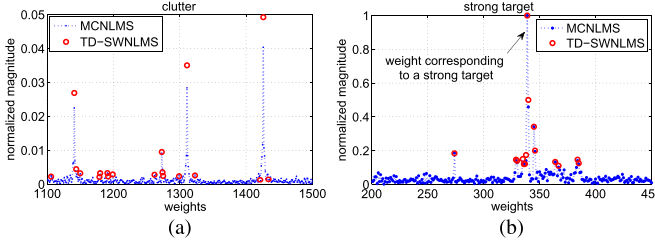


Fig. 9. Part of TD-SWNLMS and MCNLMS filter weights. (a) Corresponding to clutter. (b) Corresponding to a strong target.

To clearly show the sparse weight characteristics of the TD-SWNLMS, a portion of the weights corresponding to the clutter and a strong target after applying the TD-SWNLMS and MCNLMS algorithms are shown in Fig. 9. It is thus clear that the weights of the proposed TD-SWNLMS filter achieve a good agreement with the distribution of multipath components and strong target echoes.

## V. CONCLUSION

A novel TD-SWNLMS filtering scheme was proposed. The proposed method was derived by extending the NLMS filter to a 2-D structure that accounts for both time delay and Doppler frequency. The weight vector is adaptively adjusted based on the sparse distribution of the multipath components and strong target echoes. Compared with the traditional NLMS filter, the sparse structure of the TD-SWNLMS better matches the distribution of multipath components and strong targets and, as such, significantly improves the interference cancellation performance. Its effectiveness was verified using real radar data.

## APPENDIX

*Derivation of (7):* Based on the principle of minimum disturbance [8], the design criterion of the TD-SWNLMS filter is a constrained optimization problem that minimizes the Euclidean norm of  $\Delta\mathbf{w}_d(n+1) = \mathbf{w}_d(n+1) - \mathbf{w}_d(n)$  subject to the following constraint:

$$\begin{aligned} y(n) &= \sum_{d=-D}^D \mathbf{w}_d^H(n+1) \mathbf{u}_d(n) \\ &= \sum_{d=-D}^D [\mathcal{P}_d^T \odot \bar{\mathbf{w}}_d^H(n+1)] [\mathcal{P}_d \odot \bar{\mathbf{u}}_d(n)]. \end{aligned} \quad (12)$$

The cost function based on the method of Lagrange multipliers is given by

$$\begin{aligned} J_d(n) &= \|\mathbf{w}_d(n+1) - \mathbf{w}_d(n)\|^2 \\ &+ \text{Re} \left\{ \bar{\lambda}^* \left[ y(n) - \sum_{d=-D}^D \mathbf{w}_d^H(n+1) [\mathcal{P}_d \odot \bar{\mathbf{u}}_d(n)] \right] \right\} \end{aligned} \quad (13)$$

where  $\bar{\lambda}$  is the complex Lagrange multiplier and  $\text{Re}\{\cdot\}$  denotes the real part operator. By setting the partial derivative of  $J_d(n)$  with respect to  $\mathbf{w}_d(n+1)$  to zero, we obtain the optimum weight vector as

$$\mathbf{w}_d(n+1) = \mathbf{w}_d(n) + \frac{1}{2} \bar{\lambda}^* \mathcal{P}_d \odot \bar{\mathbf{u}}_d(n). \quad (14)$$

Substituting (14) into (12) yields

$$\bar{\lambda} = 2 \left[ y(n) - \sum_{d=-D}^D \mathbf{w}_d^H(n) \mathbf{u}_d(n) \right] \left[ \sum_{d=-D}^D \|\mathbf{u}_d(n)\|^2 \right]^{-1}. \quad (15)$$

By substituting (15) into (14) and introducing a step size factor, we obtain

$$\mathbf{w}_d(n+1) = \mathbf{w}_d(n) + \frac{\mu_d}{\lambda' + \sum_{d=-D}^D \|\mathbf{u}_d(n)\|^2} \mathbf{u}_d(n) e^*(n). \quad (16)$$

## REFERENCES

- [1] C. J. Baker, H. D. Griffiths, and I. Papoutsis, "Passive coherent location radar systems. Part 2: Waveform properties," *Proc. Inst. Elect. Eng.—Radar Sonar Navig.*, vol. 152, no. 3, pp. 160–168, Jun. 2005.
- [2] H. D. Griffiths, C. J. Baker, H. Ghaleb, R. Ramakrishnan, and E. Willman, "Measurement and analysis of ambiguity functions of off-air signals for passive coherent localisation," *Electron. Lett.*, vol. 39, no. 13, pp. 1005–1007, Jun. 2003.
- [3] A. Lauri, F. Colone, R. Cardinali, and P. Lombardo, "Analysis and emulation of FM radio signals for passive radar," in *Proc. IEEE Conf. Aerosp.*, Mar. 2007, pp. 3–10.
- [4] S. R. J. Axelsson, "Improved clutter suppression in random noise radar," in *Proc. URSI Commission F Symp. Microw. Remote Sens. Earth, Oceans, Ice, Atmos.*, Apr. 2005.
- [5] K. S. Kulpa and Z. Czekala, "Masking effect and its removal in PCL radar," *Proc. Inst. Elect. Eng.—Radar Sonar Navig.*, vol. 152, no. 3, pp. 174–178, Jun. 2005.
- [6] P. E. Howland, D. Maksymiuk, and G. Reitsma, "FM radio based bistatic radar," *Proc. Inst. Elect. Eng.—Radar Sonar Navig.*, vol. 152, no. 3, pp. 107–115, Jun. 2005.
- [7] M. Mateusz, "Comparison of adaptive methods for clutter removal in PCL radar," in *Proc. Int. Radar Symp.*, May 2006, pp. 1–4.
- [8] S. Haykin, *Adaptive Filter Theory*, 4th ed. Englewood Cliffs, NJ, USA: Prentice-Hall, 2002.
- [9] F. Colone, R. Cardinali, and P. Lombardo, "Cancellation of clutter and multipath in passive radar using a sequential approach," in *Proc. IEEE Conf. Radar*, Apr. 2006, pp. 393–399.
- [10] F. Colone, D. W. O'hagan, P. Lombardo, and C. J. Baker, "A multistage processing algorithm for disturbance removal and target detection in passive bistatic radar," *IEEE Trans. Aerosp. Electron. Syst.*, vol. 45, no. 7, pp. 698–722, Apr. 2009.
- [11] M. Meller, "Cheap cancellation of strong echoes for digital passive and noise radars," *IEEE Trans. Signal Process.*, vol. 60, no. 5, pp. 2654–2659, May 2012.
- [12] X. Guan, D. H. Hu, L. H. Zhong, and C. B. Ding, "Strong echo cancellation based on adaptive block notch filter in passive radar," *IEEE Geosci. Remote Sens. Lett.*, vol. 12, no. 2, pp. 339–343, Feb. 2015.
- [13] M. Wu, T. Shan, and Z. H. Zhuo, "An adaptive filter with discrete distribution structure in DTV based passive radar," in *Proc. Int. Conf. Instrum., Meas., Comput., Commun. Control*, Oct. 2011, pp. 755–758.
- [14] T. Shan, Y. H. Ma, R. Tao, and S. H. Liu, "Multi-channel NLMS-based sea clutter cancellation in passive bistatic radar," *IEICE Electron. Exp.*, vol. 10, no. 20, pp. 1–12, Oct. 2014.